Dalton Transactions

Macrocycle- and metal-centered reduction of metal tetraphenylporphyrins where metal is copper(II), nickel(II) and iron(II)

Journal:	*Dalton Transactions*
Manuscript ID	DT-ART-08-2021-002573.R2
Article Type:	Paper
Date Submitted by the Author:	22-Sep-2021
Complete List of Authors:	Nazarov, Dmitry; Institute of Problems of Chemical Physics RAS Andronov, Mikhail ; Institute of Problems of Chemical Physics RAS, Chernogolovka, Moscow region, 142432 Russia, Kinetics and Catalysis; Moscow State University, Leninskie Gory,119991 Moscow, Russia Kuzmin, Alexey; Institute of Solid State Physics RAS, Khasanov, Salavat; Institute of Solid State Physics RAS, Yudanova, Evgeniya; Institute of Problems of Chemical Physics RAS, Shestakov, Alexander; Institute of Problems of Chemical Physics RAS Otsuka, Akihiro; Kyoto University - Yoshida Campus, Department of Chemistry; Research Center for Low Temperature and Materials Sciences Yamochi, Hideki; Kyoto University, Division of Chemistry in Graduate School of Science Kitagawa, Hiroshi; Kyoto University, Department of Chemistry Konarev, Dmitri; Institute of Problems of Chemical Physics RAS,

ARTICLE

Macrocycle- and metal-centered reduction of metal tetraphenylporphyrins where metal is copper(II), nickel(II) and iron(II)†

Received 00th January 20xx,
Accepted 00th January 20xx

DOI: 10.1039/x0xx00000x

Dmitry I. Nazarov,[a] Mikhail G. Andronov,[a, b] Aleksey V. Kuzmin,[c] Salavat S. Khasanov,[c] Evgeniya I. Yudanova,[a] Alexander F. Shestakov,[a,b] Akihiro Otsuka,[d, e] Hideki Yamochi,[d, e] Hiroshi Kitagawa,[d] and Dmitri V. Konarev*[a]

Reduction of metal(II) tetraphenylporphyrins, where metal(II) is copper, nickel or iron, has been performed in toluene solution in the presence of a cryptand. Cesium anthracenide was used as a reductant. Crystalline salts $\{cryptand(Cs^+)\}_2\{Cu^{II}(TPP^{4-})\}^{2-}$ (**1**) and $\{cryptand(Cs^+)\}\{Ni^{I}(TPP^{2-})\}^{-}\cdot C_6H_5CH_3$ (**2**) have been obtained. Two-electron reduction of $\{Cu^{II}(TPP^{2-})\}^0$ is centered on the macrocycle allowing one to study for the first time structure and properties of the TPP^{4-} tetraanions in solid state. Tetraanions have diamagnetic state and show essential C-C_{meso} bond alternation. New bands attributed to TPP^{4-} appear at 670, 770 and 870 nm. Unpaired S = 1/2 spin is localized on Cu^{II}. One-electron reduction of $\{Ni^{II}(TPP^{2-})\}^0$ centered on nickel provides the formation of $\{Ni^{I}(TPP^{2-})\}^-$ with unpaired S = 1/2 spin localized on Ni^{I} at 100(2) K. Effective magnetic moment of **2** is 1.68 μ_B at 120 K and a broad asymmetric EPR signal characteristic of Ni^{I} is observed for **2** and also for **3** in the 4.2-120 K range. Since dianionic TPP^{2-} macrocycles are present at 100(2) K, no alternation of C-C_{meso} bonds is observed in **2**. Excited quartet S = 3/2 state according to the calculations is positioned close to the ground S = 1/2 state. In the excited state, charge transfer from Ni^{I} to the macrocycle takes place providing the formation of Ni^{II} with S = 1 and $TPP^{\bullet 3-}$ with S = 1/2 in the $\{Ni^{II}(TPP^{\bullet 3-})\}^-$ anions. Therefore, the increase in magnetic moment of **2** above 150 K is attributed to population of the excited quartet state with a gap of 750 K. Salt **2** is EPR silent above 150 K and manifests absorption bands characteristic of $TPP^{\bullet 3-}$ at RT. Reduction of $Ni^{II}(TPP^{2-})$ and $Fe^{II}(TPP^{2-})$ by cesium anthracenide in the presence of Bu_3MeP^+ yields crystals of $(Bu_3MeP^+)\{Ni^{I}(TPP^{2-})\}^-\cdot C_6H_5CH_3$ (**3**) and $(Bu_3MeP^+)\{Fe^{I}(TPP^{2-})\}^-\cdot C_6H_5CH_3$ (**4**) whose crystal structures and optical properties are also presented. DFT calculations have been carried out for $\{M^{II}(TPP^{2-})\}$ (M = Cu, Ni and Fe) and their anions to interpret experimental results obtained for **1**-**4**.

Introduction

Metal complexes of porphyrins are of importance for life on the Earth.[1] Due to unique electronic structure, they are used as dyes, catalysts and promising materials for electronics and solar cells.[2] Oxidation or reduction of metal macrocycles can affect their magnetic, optical and conducting properties due to unpaired electrons generated on the macrocycles. Metal atoms can participate in magnetic coupling of spins or high conductivity.[3] Oxidized metalloporphyrins have been studied for a long time.[4] Reduction of metalloporphyrins is hindered because of their low reduction potentials (E_{redox} < -1.2 V)[5]. Therefore, both strong reductants and pure solvents, and atmosphere free of traces of

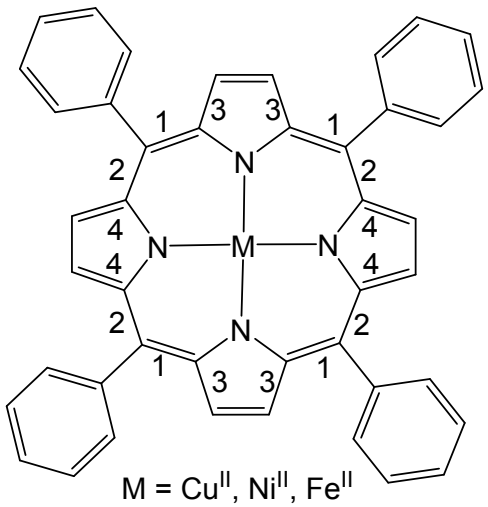

Scheme 1. Molecular structure of metal(II) tetraphenylporphyrins, M^{II}(TPP) studied in this work. Numbers are given for Table 2.

[a] *Institute of Problems of Chemical Physics RAS, Chernogolovka, Moscow region, 142432 Russia, E-mail: konarev3@yandex.ru;*
[b] *Moscow State University, Leninskie Gory,119991 Moscow, Russia;*
[c] *Institute of Solid State Physics RAS, Chernogolovka, Moscow region, 142432 Russia;*
[d] *Division of Chemistry, Graduate School of Science, Kyoto University, Sakyo-ku, Kyoto 606-8502, Japan;*
[e] *Research Center for Low Temperature and Materials Sciences, Kyoto University, Sakyo-ku, Kyoto 606-8501, Japan*

†Electronic Supplementary Information (ESI) available: IR spectra of starting compounds and salts **1-4**, UV-visible-NIR spectrum of **3**, crystal structures of **1-4**, additional magnetic data for **1** and **2**, results of theoretical calculations and xyz files for calculated structures. See DOI: 10.1039/x0xx00000x

oxygen and water should be used. As a result, experiments with negatively charged porphyrins and metal porphyrins are limited mainly by electrochemistry in solution, and many aspects of metal porphyrin chemistry of negatively charged ions remain veiled in solid state. Recently, first crystalline salt with radical anions of free-base tetra(4-pyridyl)porphyrin has been obtained using a strong reductant - potassium graphite in the presence of cryptand[2.2.2].[6] Salts with radical anions of free-base tetrakis(pentafluorophenyl)porphyrin and tetraphenylporphyrin have also recently been investigated in crystalline state. In the latter case even stronger reductant cesium anthracenide is used in toluene to reduce porphyrins.[7] Some metal porphyrins with radical trianionic and tetraanionic macrocycles are known, namely, reduced aluminum(III) or silicon(IV) tetraphenylporphyrins which can be obtained as formally neutral compounds: $\{Al^{III}(THF)_2(TPP^{\bullet 3-})\}^{\bullet}$ and $\{Si^{IV}(THF)_2(TPP^{4-})\}$.[8] However, salts containing discrete radical anions or dianions of metal porphyrins are not investigated in solid state so yet.

In this work a series of metal tetraphenylporphyrins (M(TPP), Scheme 1) where metal is copper(II), nickel(II) and iron(II) is reduced by cesium anthracenide in toluene in the presence of cryptand[2.2.2] (abbreviation is cryptand) or organic cation - tributylmethylphosphonium (Bu_3MeP^+). Crystalline salts have been obtained in high yield in the case of cryptand allowing one to study not only the crystal structures of $\{cryptand(Cs^+)\}_2\{Cu^{II}(TPP^{4-})\}^{2-}$ (**1**) and $\{cryptand(Cs^+)\}\{Ni^{I}(TPP^{2-})\}^{-}\cdot C_6H_5CH_3$ (**2**) but their solid state optical and magnetic properties as well. It is first characterization of the $\{Ni^{I}(TPP^{2-})\}^{-}$ anion in solid state which shows an unusual temperature-induced transition from doublet- to quartet-spin state accompanied by electron transfer from Ni^{I} to the macrocycle. The $\{Cu^{II}(TPP^{4-})\}^{2-}$ dianions which are formed at extremely negative reduction potentials have also been studied for the first time. Salts $(Bu_3MeP^+)\{Ni^{I}(TPP^{2-})\}^{-}\cdot C_6H_5CH_3$ (**3**) and $(Bu_3MeP^+)\{Fe^{I}(TPP^{2-})\}^{-}\cdot C_6H_5CH_3$ (**4**) have been obtained as crystals allowing their crystal structures and optical properties to be studied. Obtained data are discussed taking into account the results of DFT calculations.

Results and discussion

a. Synthesis.

Table 1. Composition of the obtained salts.

N	Composition
1	$\{cryptand(Cs^+)\}_2\{Cu^{II}(TPP^{4-})\}^{2-}$
2	$\{cryptand(Cs^+)\}\{Ni(TPP)\}^{-}\cdot C_6H_5CH_3$
3	$(Bu_3MeP^+)\{Ni(TPP)\}^{-}\cdot C_6H_5CH_3$
4	$(Bu_3MeP^+)\{Fe^{I}(TPP^{2-})\}^{-}\cdot C_6H_5CH_3$

Metal-free and metal-containing porphyrins have negative first reduction potentials at -1.26- -1.28 V *vs* SCE in CH_2Cl_2 for H_2TPP, $Cu^{II}(TPP^{2-})$ and $Ni^{II}(TPP^{2-})$.[9] Second reduction of $Cu^{II}(TPP^{2-})$ is observed at -1.72 V *vs* SCE in CH_2Cl_2[9b] indicating that these dianions are extremely air-sensitive. Previously we have found that potassium graphite is a too weak donor to be used for preparation of a radical anion salt of H_2TPP. In this case a stronger reductant cesium anthracenide $(Cs^+)(C_{14}H_{10}^{\bullet-})$ was used. Anthracenide radical anions are oxidized at -1.98 V (in 96% dioxane, 4% H_2O; *vs* SCE).[10] These radical anions are unstable in *o*-dichlorobenzene due to reduction of this solvent but stable in toluene for a long time. Taking into account reduction potentials of metal(II) tetraphenylporphyrins, this reductant is suitable for selective generation of their mono- or dianions. Amount of cesium anthracenide dissolved in toluene can be regulated by using cryptand. It forms stable $\{cryptand(Cs^+)\}$ cations dissolving appropriate amount of $C_{14}H_{10}^{\bullet-}$. These cations provide high enough solubility of both mono- and dianion salts of metal tetraphenylporphyrins in toluene allowing salts **1** and **2** to be obtained as crystals in high yield (Table 1). Additionally we have studied the reduction of metal tetraphenylporphyrins by cesium anthracenide in the presence of organic tributylmetylphosphonium cations (Bu_3MeP^+). Previously these cations have been used successfully to obtain crystalline salts with dianions of metal-oxo complexes of phthalocyanines[11] or radical anions of aromatic hydrocarbon decacyclene[12]. Indeed, salts of metal(II) tetraphenylporphyrins with Bu_3MeP^+ can also be obtained but their solubility is rather low in toluene. Similar behavior has been found previously for radical anion salts of decacyclene. Salt $\{cryptand(Cs^+)\}(decacyclene^{\bullet-})$ is well soluble in toluene and is obtained in high yield but salt $(Bu_3MeP^+)(decacyclene^{\bullet-})$ has low solubility allowing one to obtain only several high quality single crystals.[11] In case of metal(II) tetraphenylporphyrins, their singly reduced salts are also only weakly soluble. As a result, crystals of **3** and **4** (Table 1) have also been obtained in low yield. Crystals belong to one crystal phase allowing one to study their crystal structures and optical properties.

b. Crystal structures.

Structure of $\{cryptand(Cs^+)\}_2\{Cu^{II}(TPP^{4-})\}^{2-}$ (**1**) was studied at 100(2) K at slow crystal cooling in a nitrogen flow. Salt has a $\{cryptand(Cs^+)\}$: CuTPP = 2 : 1 ratio and, hence, metal porphyrin is in dianion state. There are two independent $\{Cu^{II}(TPP^{4-})\}^{2-}$ dianions in **1** which have different cationic surrounding, and cesium cations approach the porphyrin plane. Previously it has been shown[7] that the $\{cryptand(Cs^+)\}$ cations can have two conformations with cesium ion positioned exactly in the center of cryptand or displaced out of cryptand approaching closely the porphyrin plane. Two Cs^+ ions approach very close the plane of one $\{Cu^{II}(TPP^{4-})\}^{2-}$ dianion (type A) with the distances between Cs^+ and the 24-atom porphyrin plane of 3.119 and 3.125 Å (Fig. 1a). Another $\{Cu^{II}(TPP^{4-})\}^{2-}$ dianion (type B) is also surrounded by two $\{cryptand(Cs^+)\}$ cations but these cations have different conformations since one Cs^+ ion is displaced out of cryptand but another Cs^+ ion is positioned exactly in the center of cryptand (Fig. 1b). As a result, the distances between two Cs^+ ions and the 24-atom porphyrin plane are different (3.037 and 5.393 Å). Nevertheless, such difference in the cationic surrounding of two $\{Cu^{II}(TPP^{4-})\}^{2-}$ cannot provide charge disproportionation (*vide infra*). This situation is different from that for H_2TPP salt. The salt of $\{cryptand(Cs^+)\}$ with $H_2TPP^{\bullet-}$ has very close approach of two Cs^+ ions (the Cs^+ - TPP plane distances are 2.83-2.86 Å) to one radical anion and far position from both Cs^+ ions for another radical anion (the shortest Cs^+ - TPP plane distance is longer than 6.92 Å). In this case charge disproportionation is observed in $\{cryptand(Cs^+)\}\{H_2TPP^{\bullet-}\}$.[7] As

for $\{Cu^{II}(TPP^{4-})\}^{2-}$, porphyrin planes are planar in both dianions in **1** but copper atoms displace slightly out of the 24-atom porphyrin plane by 0.003 and 0.050 Å. Since Cs^+ ions also approach close the Cu^{II} atoms, different cationic surrounding of the Cu^{II} atoms can provide slightly different displacement of copper atoms from the porphyrin plane. The $(Cs^+)\cdots(Cu^{II})$ contacts are about 3.60 and 3.45 Å for the dianions of type A and B, respectively (Figs. 1a and 1b). The Cu^{II} atom forms four short Cu-N bonds with average length of 2.005(1) Å in pristine $\{Cu^{II}(TPP^{2-})\}^0$. Addition of two electrons to the macrocycle elongates these bonds to 2.026-2.029(2) Å for two independent dianions in **1**. Elongation of these bonds by 0.021-0.024 Å shows essential destabilization of the Cu^{II}-N bonds under reduction. Another interesting feature of **1** is the appearance of alternation of C_{meso}-C bonds (bonds of type 1 and 2 in Scheme 1) and C-C bonds in the pyrrole rings (bonds of type 3 and 4 in Scheme 1). Shortened and elongated bonds are positioned in such a way that they belong to two oppositely located pyrrole rings. The formation of longer C_{meso}-C bonds is accompanied by the formation of shorter C-C bonds in the same pyrrole ring and *vice versa*. Alternation is not uniform for two independent $\{Cu^{II}(TPP^{4-})\}^{2-}$ dianions. For the dianion with symmetric cationic surrounding (type A), the difference between longer and shorter bonds is 0.024 and 0.014 Å for the C_{meso}-C bonds and the C-C bonds in the pyrrole rings, respectively (Table 2). The same differences for the dianion with asymmetric surrounding (type B) are noticeably greater being 0.069 and 0.053 Å, respectively (Table 2). Obviously, cationic surrounding affects alternation of the bonds in the TPP^{4-} macrocycles. Aromatic 18 π-electron TPP^{2-} macrocycle has no alternation of bonds but such alternation appears in less aromatic 19 or 20 π-electron systems of $TPP^{\bullet 3-}$ or TPP^{4-}, respectively, due to partial loss of macrocycle aromaticity.[6-8] Previously[11] it has been shown that alternation of the N_{meso}-C bonds is stronger for the $\{M^{IV}O(Pc^{4-})\}^{2-}$ dianions (0.066-0.082 Å) as compared with the $\{M^{IV}O(Pc^{\bullet 3-})\}^{\bullet -}$ radical anions (0.025-0.036 Å) (M = Ti or V). Crystal structure of **1** is shown in Fig. S5a. It is seen that both $\{Cu^{II}(TPP^{4-})\}^{2-}$ dianions are isolated by bulky $\{cryptand(Cs^+)\}$ cations.

Crystal structures of $\{cryptand(Cs^+)\}\{Ni^{I}(TPP^{2-})\}^{-}\cdot C_6H_5CH_3$ (**2**) and $(Bu_3MeP^+)\{Ni^{I}(TPP^{2-})\}^{-}\cdot C_6H_5CH_3$ (**3**) with the $\{Ni^{I}(TPP^{2-})\}^{-}$ anions have been studied at low temperature (100(2) K) after slow cooling of crystals. The salts contain well-ordered components including solvent $C_6H_5CH_3$ molecules, and only butyl substituents of Bu_3MeP^+ are disordered. Attempts to solve these crystal structures at higher temperatures (for example, at 250 K) were unsuccessful due to strong disorder of solvent molecules together with cations. There is only one independent $\{Ni^{I}(TPP^{2-})\}^{-}$ anion in **2** and **3**. The Cs^+ ions are displaced out of cryptand closely approaching the porphyrin surface. The shortest distance between the Cs^+ ion and 24-atom p

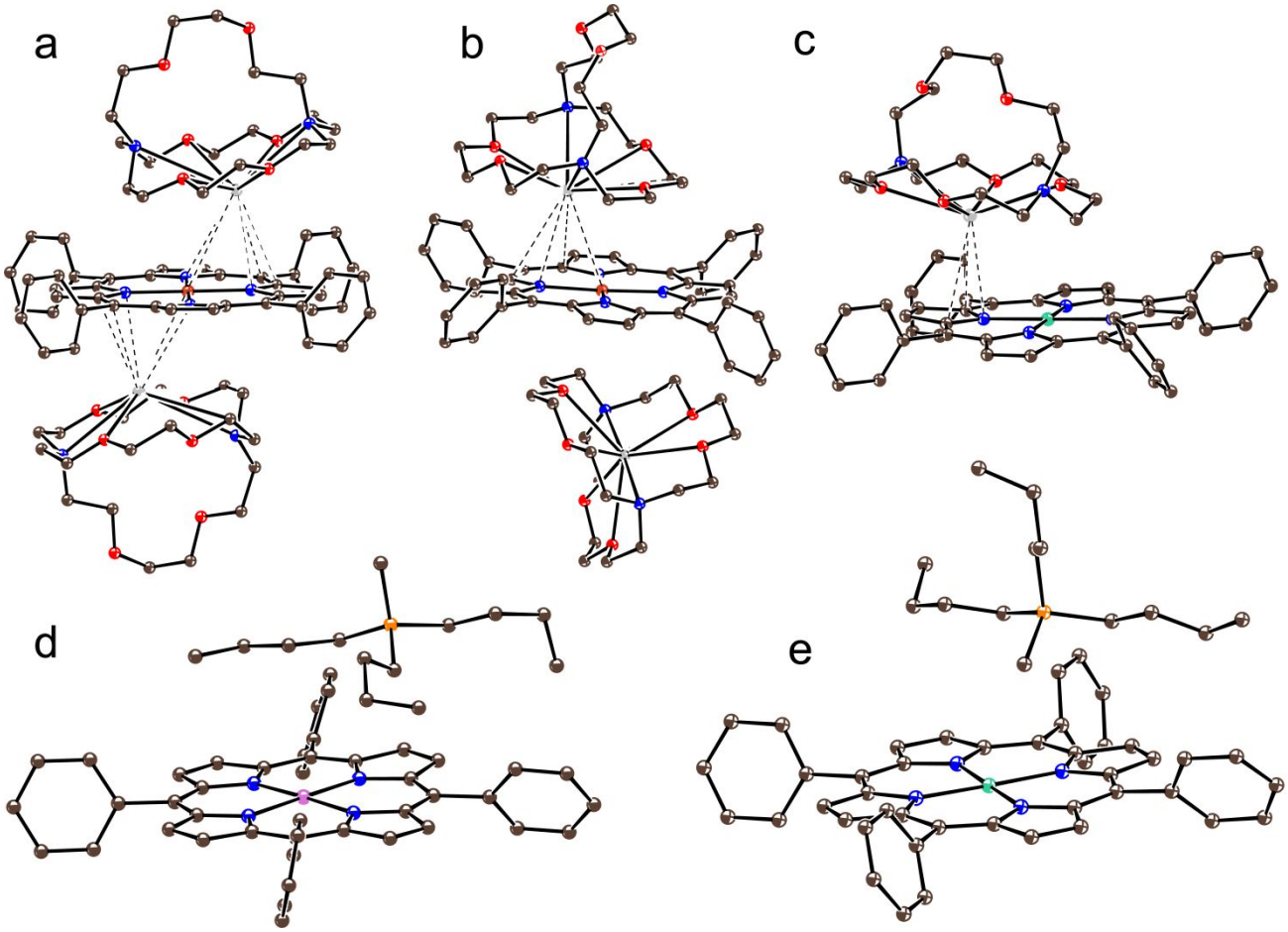

Figure 1. Molecular structures of: $\{Cu^{II}(TPP^{4-})\}^{2-}$ type A (a) and B (b) in $\{cryptand(Cs^+)\}_2\{Cu^{II}(TPP^{4-})\}^{2-}$ (**1**); (c) $\{cryptand(Cs^+)\}_2\{Ni^{I}(TPP^{2-})\}^{-}$ unit in **2**; (d) $(Bu_3MeP^+)\{Fe^{I}(TPP^{2-})\}^{-}$ unit in **4**; and (e) $(Bu_3MeP^+)\{Ni^{I}(TPP^{2-})\}^{-}$ unit in **3**. Short contacts between cesium ions and porphyrins are shown by dashed lines.

Table 2. Bond lengths in the tetraphenylporphyrin macrocycles in pristine compounds and salts **1**-**4**. Types of bonds are given according to Scheme 1.

Compound	Average bond length, Å						
	M-N	1	2	Difference 2-1	3	4	Difference 4-3
$Cu^{II}(TPP^{2-})$ at 120 K[14]	2.005(1)	1.394(3)		0	1.440(3)		0
$\{Cu^{II}(TPP^{4-})\}^{2-}$ in **1**							
type A	2.029(2)	1.416(4)	1.392(4)	0.024	1.431(4)	1.417(4)	0.014
type B	2.026(2)	1.441(4)	1.372(4)	0.069	1.449(4)	1.398(4)	0.053
$Ni^{II}(TPP^{2-})$ at RT[13]	1.931(1)	1.384(3)		0	1.428(3)		0
$\{Ni^{I}(TPP^{2-})\}^{-}$ in **2**	2.005(1)	1.397(2)	1.395(2)	0.002	1.441(2)	1.439(2)	0.003
$\{Ni^{I}(TPP^{2-})\}^{-}$ in **3**	2.008(2)	1.401(4)	1.397(4)	0.004	1.441(4)	1.439(4)	0.003
$Fe^{II}(TPP^{2-})$ at 120 K[15]	1.966(1)	1.395(3)		0	1.439(3)		0
$\{Fe^{I}(TPP^{2-})\}^{-}$ in **4**	1.980(3)	1.397(5)	1.387(5)	0.010	1.430(5)	1.425(5)	0.005

porphyrin plane is 3.23 Å in **2**. This distance is longer in comparison with **1** due to decreased electrostatic interaction of Cs^+ with monoanions in **2** in comparison with dianions in **1**. Short average Ni^{II}-N bonds of 1.931(1) Å length are characteristic of pristine $\{Ni^{II}(TPP^{2-})\}^0$ (Table 2).[13] Reduction elongates these bonds up to 2.005-2.008(2) Å (Table 2). Elongation of the bonds by 0.074-0.077 Å is essentially greater than that in **1** and can be most probably explained by the formation of Ni^{I}. Thus, single reduction destabilizes nickel-nitrogen bonding. Porphyrin macrocycles are planar in both **2** and **3.** It should be noted that hydrogen atom of {cryptand(Cs^+)} closely approaches the nickel atom in **2** (the Ni···H distance is 2.70 Å), and nickel atom is displaced out of the 24-atom porphyrin plane towards this hydrogen atom by about 0.005 Å. Hydrogen atom of Bu_3MeP^+ cation closely approaches the nickel atom with the Ni···H distance of 2.60 Å in **3**. In this case even stronger displacement of nickel atoms from the 24-atom porphyrin plane towards this hydrogen is observed (0.017 Å). The C_{meso}-C and the C-C bonds in the pyrrole rings do not alternate in both salts since the difference between shorter and longer bonds of 0.002-0.004 Å is within the error for the determination of these bond lengths (0.003 Å). The absence of alternation is observed in pristine $Ni^{II}(TPP^{2-})$ containing dianionic TPP^{2-} macrocycle (Table 2). All these data indicate metal-centered reduction of starting $\{Ni^{II}(TPP^{2-})\}^0$ and the formation of the $\{Ni^{I}(TPP^{2-})\}^{-}$ anions in both **2** and **3** at 100(2) K. Views on the crystal structures of **2** and **3** are shown in Figs. S5b and S6a, respectively. The $\{Ni^{I}(TPP^{2-})\}^{-}$ anions alternate along the *b* axis with the {cryptand(Cs^+)} cations in **2** (Fig. S5b) and Bu_3MeP^+ cations in **3** (Fig. S6a). The $\{Ni^{I}(TPP^{2-})\}^{-}$ monoanions are isolated in both salts since all C···C contacts between them exceed 3.55 Å.

It is well known[16, 17] that reduction of iron(II) phthalocyanine is metal-centered providing the formation of the $\{Fe^{I}(Pc^{2-})\}^{-}$ anions with *S* = 1/2 spin state for iron(I). This conclusion can be made from the absence of alternation of the N_{meso}-C bonds and any absorption bands at 900-1100 nm characteristic of $Pc^{\bullet 3-}$. In some cases EPR signal characteristic of Fe^{I} can be found in the salts. Such behavior is observed in solution[16] and solid state[17]. Hexadecachlorosubstituted iron(II) phthalocyanine shows similar behaviour[18] whereas substituted iron(II) tetrapyrazinoporphyrazines with stronger acceptor properties can show both metal- and macrocycle-centered reduction.[19] Less information is known about reduced iron(II) porphyrins since only several compounds were obtained and studied in solid state. It is reported that first and second reduction of iron(II) tetraphenylporphyrin is centered on the macrocycle providing the formation of the $TPP^{\bullet 3-}$ and TPP^{4-} macrocycles, respectively, whereas iron(II) preserves its +2 charge and *S* = 1 spin state. These conclusions are based on X-ray absorption and Mössbauer spectroscopy as well as theoretical calculations.[20] X-ray diffraction data for $(Bu_3MeP^+)\{Fe^{I}(TPP^{2-})\}^{-}\cdot C_6H_5CH_3$ (**4**) correspond better to metal-centered reduction of $Fe^{II}TPP$ accompanied by the formation of Fe^{I} and preservation of dianionic TPP^{2-} macrocycles. This follows from only weak alternation of the C-C bonds observed in **4** (0.005-0.010 Å, Table 2), which is close to the error for determination of these bond lengths (0.005 Å, Table 2) and essentially weaker than similar alternation observed for $H_2TPP^{\bullet -}$ or $TPP^{\bullet 3-}$.[7, 8a] Reduction elongates average Fe-N bonds (by 0.014 Å) but

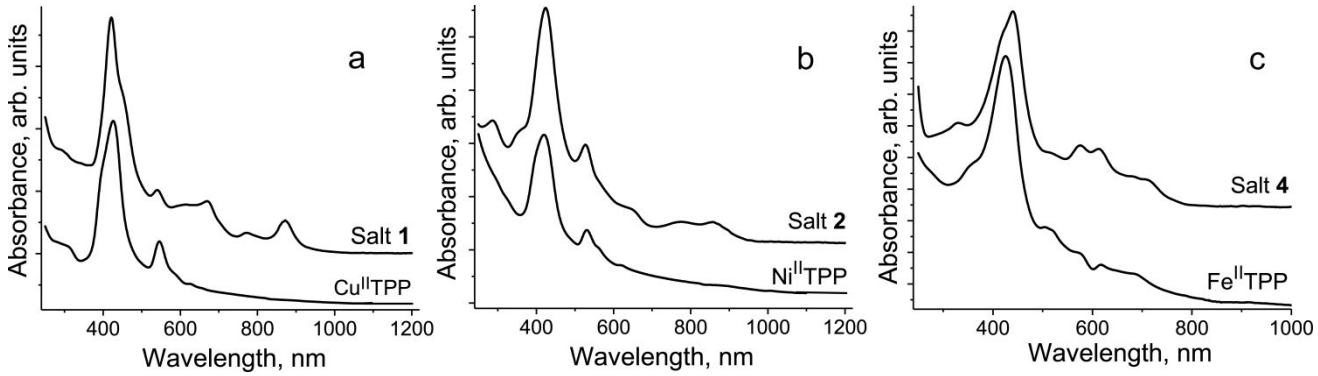

Figure 2. Spectra of pristine metalloporphyrins and salts **1**, **2** and **4**: (a) $Cu^{II}(TPP^{2-})$ and salt **1**; (b) $Ni^{II}(TPP^{2-})$ and salt **2** (salt **3** has similar spectrum shown in Fig. S7) and (c) $Fe^{II}(TPP^{2-})$ and salt **4** in KBr pellets. Pellets were prepared in strictly anaerobic conditions.

this elongation is smaller than those for reduced nickel(II) and copper(II) tetraphenylporphyrins studied in this work. It should be noted that reduction of $Fe^{II}Pc$ also shortens average Fe-N bonds by 0.01-0.02 Å[17-19]. Iron(I) atom in **4** displaces slightly out of the porphyrin plane by 0.024 Å towards hydrogen atom of butyl substituent of the neighboring Bu_3MeP^+ cation. Crystal structure of **4** is similar to that of **3** with alternation of the Bu_3MeP^+ and $\{Fe^{I}(TPP^{2-})\}^-$ ions along the *b* axis, and there are no shortened contacts between the $\{Fe^{I}(TPP^{2-})\}^-$ anions (Fig. S6b).

c. Optical properties.

Spectra of pristine metalloporphyrins (M = Cu^{II}, Ni^{II}, Fe^{III}) contain a Soret band at 300-460 nm and Q-bands of relatively weak intensity in the visible range (with maxima at 500-680 nm) (Table S2). Reduction of substituted metal-free porphyrins shifts slightly the Soret band to lower energies and preserves or even increases the number of Q-bands which generally are only slightly shifted. New NIR bands appear at 750-900 nm as well.[6,7] The appearance of the latter bands is a very important sign of macrocycle reduction since partial or full population of the LUMO in $H_2(porphyrin)^{\bullet-}$ allows new transitions from this LUMO to the above located orbitals. Reduction of metalloporphyrins shows similar tendencies. The Soret band nearly preserves its position in the spectrum of **1** but a new band is manifested as a shoulder at about ~450 nm (Fig. 2a). One higher-energy Q-band preserves its position but two new Q-bands appear at 615 and 670 nm (Fig. 2a). Two new bands are also manifested in the NIR range at 770 and 870 (maximum) nm that unambiguously justifies macrocycle reduction and population of LUMO of the macrocycle. Spectra of **2** (Fig. 2b) and **3** (Fig. S7) are similar. The formation of **2** and **3** is accompanied by slight blue shift of both Soret and Q bands (Table S2). The appearance of new bands at 772-774 and 850-854 (maximum) nm (Figs. 2b and S7) justifies that LUMO of the macrocycle is populated at room temperature (295 K, temperature for measurements of the UV-visible-NIR spectrum). This interpretation is in contradiction with X-ray diffraction data obtained at 100(2) K which show dianionic 2– state of the macrocycle. One of reasons can be electron transfer from Ni^{I} to TPP^{2-} realized above 100 K and accompanied by the formation of Ni^{II} and $TPP^{\bullet3-}$ as described in the next section.

Reduction of $\{Fe^{II}(TPP^{2-})\}$ is accompanied by slight red shift of the Soret band in the spectrum of **4** (Table S2). Four Q-bands are also manifested in the spectrum of **4**, and some of them are noticeably red-shifted (Fig. 2c, Table S2). However, the spectrum of **4** is different from those of **1** and **2** due to the absence of any NIR bands of $TPP^{\bullet3-}$ in the 750-900 nm range (Fig. 2c). Preservation of TPP^{2-} confirms metal-centered reduction of $\{Fe^{II}(TPP^{2-})\}^0$ supposed from the X-ray diffraction data.

IR-spectra of $\{M^{II}(TPP^{2-})\}^0$ and salts **1** - **4** are shown in Figs. S1-S4, and positions of the peaks are listed in Table S1. There are several intense bands in the spectra of metalloporphyrins which are reproduced in the spectra of the salts. Intense bands at 696-700 and 741-750 cm^{-1} are shifted at the reduction to greater wavenumbers by 3-12 cm^{-1} in the spectra of **1** - **3** but they preserve initial position in the spectrum of **4** in which macrocycle is not reduced (Table S1). An intense band at 791-803 cm^{-1} is shifted to smaller wavenumbers in the spectra of **1** - **3** (this shift is maximal (24 cm^{-1}) in the spectrum of **1,** Table S1) but this shift is observed in the spectrum of **4** in the opposite direction from 803 to 820 cm^{-1}. Intensity of these bands also decreases at the formation of the salts, and this band is hardly observed in the spectrum of **1** with tetraanionic macrocycle (Fig. S1). All starting metalloporphyrins contain the most intense band at 1000-1005 cm^{-1} (Figs. S1-S4). Intensity of this band also decreases at the formation of **2**-**4,** and this band is very weak in the spectrum of **1**. The band at 1347-1352 cm^{-1} (Figs. S1-S4) is noticeably shifted by 6-14 cm^{-1} to smaller wavenumbers at the reduction but the band of $\{Fe^{II}(TPP^{2-})\}^0$ at 1068 cm^{-1} preserves the same position at reduction. Other bands of metalloporphyrins are not shifted essentially at the formation of the salts (see Table S1).

d. Magnetic properties

Magnetic properties of **1** and **2** have been studied by both SQUID magnetometer and EPR for polycrystalline samples in strictly anaerobic conditions. Only temperature dependent EPR spectra are recorded for salt **3**. Effective magnetic moment of **1** is 1.82 μ_B at 300 K (Fig. S9a) indicating a contribution of one S = 1/2 spin per formula unit (calculated value for one independent S = 1/2 spin is 1.73 μ_B). Magnetic moment is nearly temperature independent and decreases slightly below 10 K (Fig. S9a). Temperature dependence of reciprocal molar magnetic susceptibility is linear nearly in all studied temperature range allowing one to determine Weiss temperature of -0.3 K (Fig. S9b), which indicates paramagnetic behavior of **1**. This can be explained by localization of spin density on the Cu(II) atoms and long distances between them (12.9 Å, Fig. S5a).

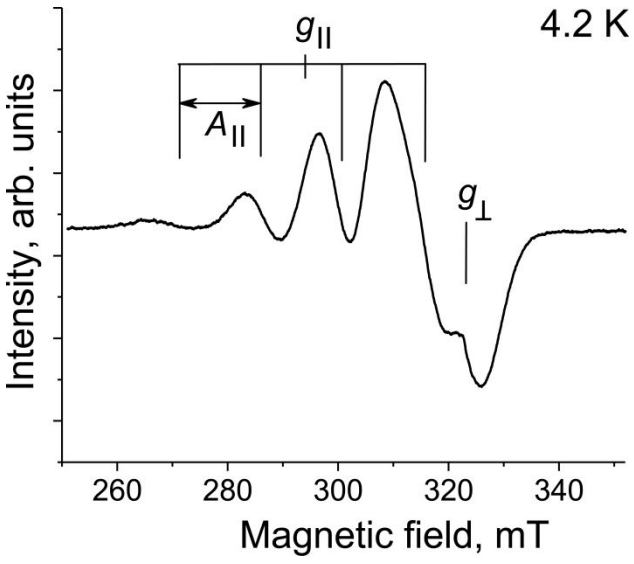

Figure 3. EPR signal from polycrystalline **1** at 4.2 K. Determination of *g*-factors and $A_{||}$ is schematically shown.

EPR spectra of **1** studied in the 295-4.2 K range support localization of unpaired spin on Cu^{II}. Spectrum at 4.2 K shown in Fig. 3 is characteristic of Cu^{II} with $g_{||}$ and $g_{\perp}$ components. The $g_{||}$ component splits into four lines due to hyperfine interaction of unpaired spin with the ^{65}Cu (I = 3/2) nucleus. Hyperfine constant $A_{||}$ is 14.69 mT at 4.2 K (Fig. 3). It should be noted that $\{Cu^{II}(Pc^{\bullet 3-})\}^{-}$, $\{Cu^{II}(F_{16}Pc^{4-})\}^{2-}$ or $\{Cu^{II}(F_8Pc^{4-})\}^{2-}$ also contain paramagnetic Cu^{II} and show EPR signals characteristic of Cu^{II}.[21] These signals also have $g_{||}$ and $g_{\perp}$ components, and four-line hyperfine splitting is observed for the $g_{||}$ component but in this case constants $A_{||}$ are in the range of 20–26 mT.[21] $g_{||}$-factor is 2.2984 at 4.2 K (Fig. 4). Component with $g_{\perp}$ has g-factor of 2.0011, and no splitting of this component is observed (Fig. 3). The absence of any signals which can be attributed to paramagnetic porphyrin species clearly shows that tetraanionic TPP^{4-} macrocycle is diamagnetic and EPR silent in **1**. Magnetic moment of **1** increases relatively the value of 1.73 μ_B indicating additional orbital contribution of the Cu^{II} ions. The value of g-factor estimated from the magnetic moment is 2.101. Spectrum of **1** at 150 K is shown in Fig. S10. Both $g_{||}$ and $g_{\perp}$ components increase slightly to $g_{||}$ = 2.2054 and $g_{\perp}$ = 2.0016 but the hyperfine constant decreases only slightly to 14.55 mT. It should be noted that a similar EPR signal is preserved in **1** up to room temperature indicating that spin is still localized exclusively on the Cu^{II} atoms.

Magnetic data for **2** are shown in Fig. 4. Effective magnetic moment of **2** is 1.76 μ_B at 150 K. This corresponds to the contribution of one S = 1/2 spin per porphyrin (calculated contribution from one non-interacting S = 1/2 spin is 1.73 μ_B). Magnetic moment is nearly temperature independent at the temperature decrease below 150 K (Fig. 4a) and the temperature dependence of reciprocal molar magnetic susceptibility is linear in the 150-7 K range. Estimated Weiss temperature of -5 K (Fig. S11b) indicates weak antiferromagnetic coupling of spins due to the absence of direct π-π interactions between $\{Ni^{I}(TPP^{2-})\}^{-}$ in **2** (Fig. S5b). EPR spectra of **2** allow one to determine where S = 1/2 spin is localized since potentially it can be arranged on the macrocycle in $\{Ni^{II}(TPP^{\bullet 3-})\}^{\bullet -}$ or on the Ni^{I} atom in $\{Ni^{I}(TPP^{2-})\}^{-}$. Both anions have close magnetic moments since in both cases only one S = 1/2 spin contributes to magnetic susceptibility. However, EPR signals from these anions should have different broadness and position. In the salts with radical anions of $H_2TPP^{\bullet -}$ a narrow EPR signal is observed which can split up to three components with the temperature decrease whose width is in the 0.2-0.6 mT range.[6, 7] The Ni^{I} atoms in the reduced tetrapyrrole macrocycles show broad asymmetric EPR signals with $g_{||}$ = 2.2 and $g_{\perp}$ = 2.05 or even three-component signals with g_x, g_y, and g_z.[22] EPR signal in **2** is observed only below 120 and down to 4.4 K (Figs. 4c and 4d). It can be fitted well by a broad line with g_1= 2.0502 and linewidth ΔH = 25.9 mT, and a narrower line

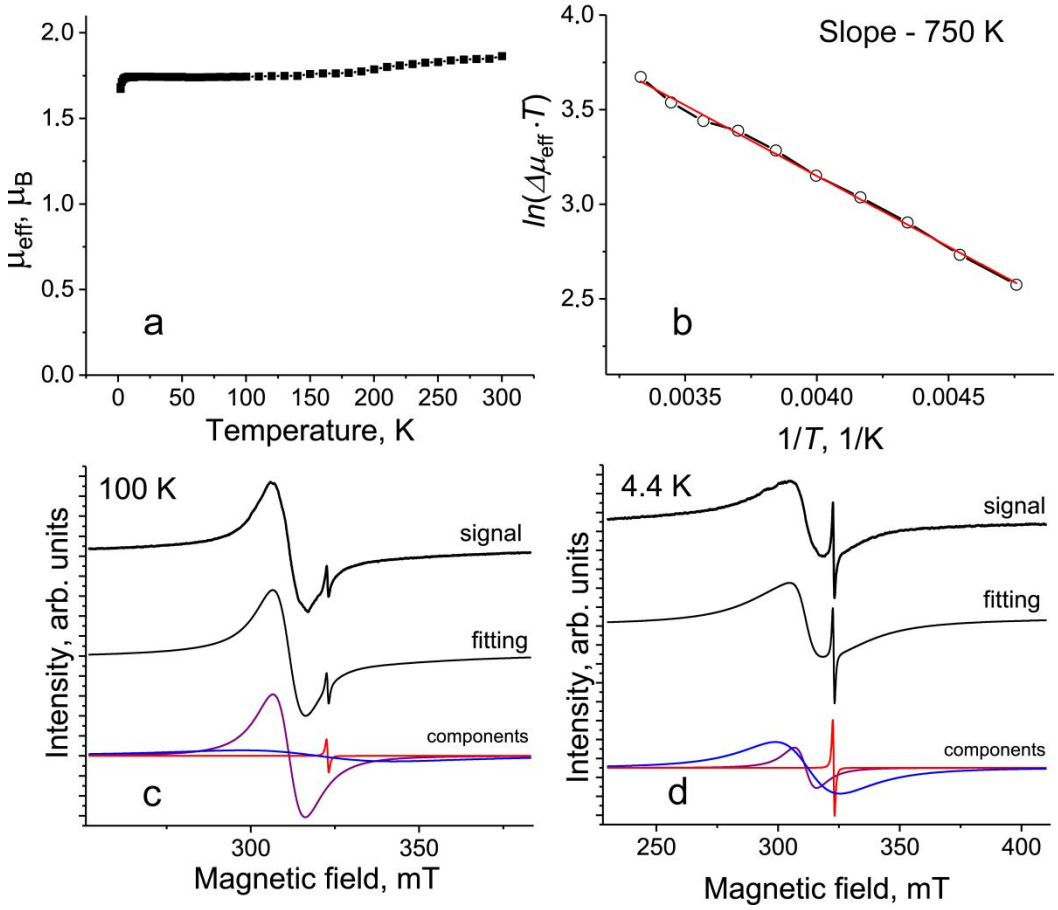

Figure 4. Magnetic data for salt $\{Crypt(Cs^{+})\}\{Ni^{I}(TPP^{2-})\}^{-}\cdot C_6H_5CH_3$ (**2**): (a) temperature dependence of effective magnetic moment and (b) the dependence of natural logarithm of changes in effective magnetic moment multiplied by temperature *vs* reverse temperature; EPR spectra of polycrystalline **2** at 100 (c) and 4.2(d) K. Fitting of the signal by three Lorentzian lines is shown below. For attribution of the lines see the text.

with g_2 = 2.0761 and ΔH = 7.265 mT at 100 K (Fig. 4c). Two components are preserved down to 4.4 K but both components are slightly narrowed, and the broader line is shifted to lower *g*-factors (Figs. S11c and S11d, respectively). As a result, the following parameters of the lines are observed at 4.4 K: g_1= 1.998, ΔH = 17.5 mT and g_2 = 2.078 and ΔH = 6.3 mT. It is seen that both components are still broad even at 4.4 K supporting our supposition that spin is localized exclusively on the Ni^{I} atoms in the 120-4.4 K range. Structure of **2** studied at 100 K also justifies the presence of TPP^{2-} and correspondingly Ni^{I} ions. A narrow component with g_3 = 2.0026, ΔH = 0.5-0.7 mT is also observed in the whole temperature range up to 295 K (Figs. 5c and 5d). This signal is very weak, and its integral intensity is less than 0.1% from that of the broad signal from Ni^{I}. It shows pure paramagnetic dependence and according to the parameters this signal can be attributed to $TPP^{\bullet 3-}$ type impurities. Effective magnetic moment increases approximately above 150 K up to 1.86 μ_B at 300 K and deviation from the Curie Weiss law is observed above this temperature (Fig. S11b). This process is temperature activated, and the plot in coordinates of natural logarithm of changes in magnetic moment multiplied by temperature *vs* reverse temperature is linear in the 210-300 K range allowing one to determine the gap between ground and excited state as 750 K (Fig. 4b). Changes in the location of the spin from Ni^{I} to $TPP^{\bullet 3-}$ potentially do not affect much magnetic moment of the complex but parameters of the EPR signal must change essentially due to narrowing of the signal and its shift to g = 2.003. However, such behavior is not observed. Since transition occurs with the increase in magnetic moment, we suppose that $\{Ni^{I}(TPP^{2-})\}^{-}$ has excited charge transfer (CT) state with $\{Ni^{II}(TPP^{\bullet 3-})\}^{-}$ ionic formula in which high-spin Ni^{II} (S = 1) and $TPP^{\bullet 3-}$ (S = 1/2) species coexist in one anion. That corresponds to the doublet-quartet transition presented in Scheme 2. Such transition can explain the disappearance of the EPR signal of **2** above 120 K since strong magnetic exchange is expected between Ni^{II} (S = 1) and $TPP^{\bullet 3-}$ (S = 1/2) to broaden the EPR signal. The presence of the absorption bands of $TPP^{\bullet 3-}$ in the optical spectrum of **2** at room temperature supports such transition. DFT calculations were carried out to estimate the possibility of doublet-quartet transition in $\{Ni^{I}(TPP^{2-})\}^{-}$ (see next section). This type of transition is rather rare. However, reduced trinickel(II)oxa trithiadodecaazahexaphyrin (Hhp) complex has been studied recently.[23] Reduction of $\{Ni^{II}_3O(Hhp^{3-})\}^{+}$ yields $\{cryptand(Cs^{+})\}_2\{Ni^{II}_2Ni^{I}O(Hhp^{5-})\}^{2-}\cdot 2C_7H_8$. Analysis of magnetic properties of these salt shows that one of three nickel(II) atoms is reduced to Ni^{I} which shows similar magnetic moment and

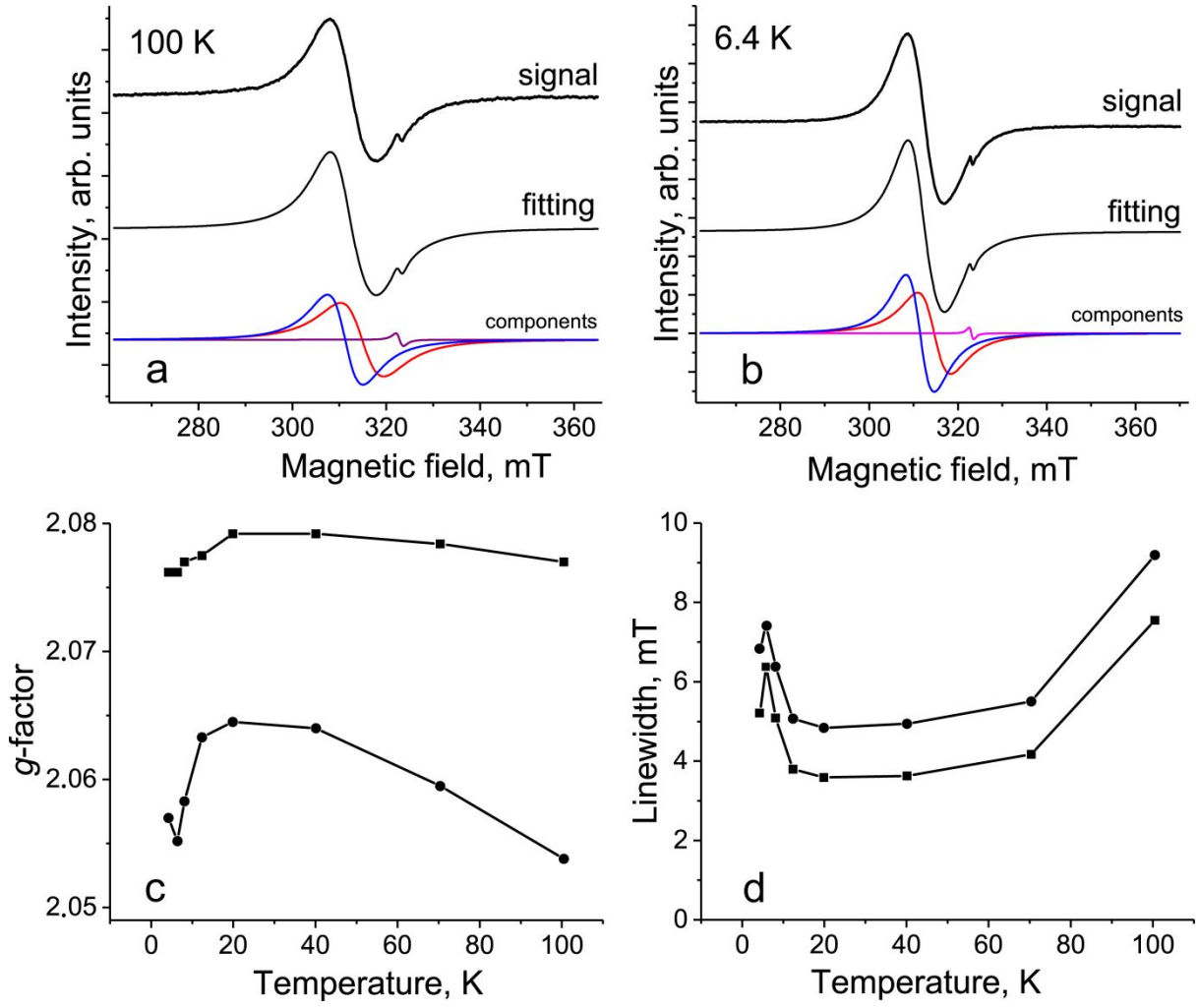

Figure 5. EPR data for salt $(Bu_3MeP^{+})\{Ni^{I}(TPP^{2-})\}^{-}\cdot C_6H_5CH_3$ (**3**): EPR signals from polycrystalline **3** at 100 (a) and 6.4 (b) K. Fitting of the signal by three Lorentzian lines is shown below. For attribution of the lines see text. Temperature dependence of *g*-factor (c) and the linewidth (d) of broad lines attributed to Ni^{I}.

EPR parameters to those of **2** below 120 K. The Hhp^{5-} macrocycle is diamagnetic but population of triplet state of this macrocycle (S = 1) is observed above 150 K. Appearance of triplets above 150 K provides disappearance of intense and broad EPR signals from Ni^{I} most probably also due to their broadening.[23] It should be noted that phenomena associated with metal to the macrocycles charge transfer have been observed previously in some metallomacrocycles.[23, 24]

Scheme 2.

$\{Ni^{I}$ (S =1/2) (Pc^{2-}) (S = 0)$\}^{-}$ ⟶ $\{Ni^{II}$ (S = 1) ($Pc^{\bullet 3-}$) (S = 1/2)$\}^{-}$

Doublet Quartet

EPR spectra of **3** were studied in the 4.2-295 K range. Salt **3** shows behavior similar to that of **2**. An intense signal appears in the spectrum of **3** below 130 K. At 100 K the broad signal can be fitted well by two lines with g_1 = 2.0713 and ΔH = 9.07 mT and g_2 = 2.0536 and ΔH = 9.07 mT (Fig. 5a). Position of these lines and their large broadness allow one to unambiguously attribute both lines to asymmetric EPR signal from Ni^{I} with $g_{\|}$ and $g_{\perp}$ components. Signal slightly narrows with the temperature decrease but below 20 K broadening of both lines is observed along with their shift to lower g-factors (Figs. 6c and 6d). As a result, two components of the EPR signal have g_1 =2.0725 and ΔH = 7.36 mT, and g_2 = 2.0561 and ΔH = 9.92 mT at 6.4 K (Fig. 5b). A weak narrow signal from $TPP^{\bullet 3-}$ is also observed in the spectrum of **3** with g_3 = 2.0024 and ΔH = 0.7-0.4 mT (Fig. 5a and 5b) but intensity of this signal is very weak (less than 0.1% from those of the broad lines). This signal can be attributed to impurities observed in the whole studied temperature range. Thus, according to EPR S = 1/2 spin in **3** is also positioned on the Ni^{I} atoms, and the transition observed approximately above 130 K is accompanied by disappearance of broad EPR signals from Ni^{I} due to CT from Ni^{I} to the macrocycle.

e. Theoretical calculations.

To understand the features of arrangement and electronic structure of tetraphenylporphyrin complexes quantum chemical calculations were carried out using PBE functional.[25] Structures of isolated $\{Ni^{II}(TPP^{2-})\}^{0}$ complex with S = 0 spin state and the $\{Ni^{I}(TPP^{2-})\}^{-}$ anions with ground S = 1/2 and excited S = 3/2 spin states are shown in Fig. S12c, S12a and S12b, respectively. The calculated bond lengths of the Ni-N and C-C bonds of the macrocycle (see Table S3) are in a good agreement with the experimental data. In this case, the difference between bonds 1 and 2, 0.010 Å, is noticeably greater than the experimental value of 0.002 Å for the complex in a crystalline environment. To elucidate the role of intermolecular Coulomb interactions on the structure of the porphyrin ligand, the structures of the neutral complex $\{(Cs^{+})[Ni^{I}(TPP^{2-})]^{-}\}$, and positively charged adducts $\{[cryptand(Cs^{+})]_2[Ni^{I}(TPP^{2-})]^{-}\}^{+}$ and $\{[Bu_3MeP^{+}]_2[Ni^{I}(TPP^{2-})]^{-}\}^{+}$ in the doublet S = 1/2 state were calculated. In all cases, under geometry optimization, the Ni-Cs or Ni-P distances were fixed as in the crystal structures of **2** and **3**. As a result, difference between the bond length of type 1 and 2 is reduced to 0.006 and 0.003 Å for $\{(Cs^{+})[Ni^{I}(TPP^{2-})]^{-}\}$ and $\{[cryptand(Cs^{+})]_2\ [Ni^{I}(TPP^{2-})]^{-}\}^{+}$, respectively. Calculations also correctly reproduce an increase in the Ni-N distance by 0.003 Å upon the transition from **2** with a cryptand cesium counterion to **3** with a phosphonium counterion.

The ground state of $\{Ni^{I}(TPP^{2-})\}^{-}$ is a doublet S = 1/2 one. As compared with the neutral complex $\{Ni^{II}(TPP^{2-})\}^{0}$, the charge on the metal atom decreases from 0.079 to 0.035. The unpaired electron is located in the x^2-y^2 orbital, which has noticeable delocalization on the ligand that leads to a decrease in spin density on the Ni atom to 0.48. In the quartet S = 3/2 state, spin density increases by 1 and the charge on the metal atom increases noticeably to 0.181. This is due to the appearance of a Ni^{II} center as a result of electron transfer from Ni^{I} to the macrocycle which should adopt the $TPP^{\bullet 3-}$ state. The difference between the energies of the S = 1/2 and S = 3/2 states is a significant value of 0.9 eV, which changes only slightly when the effect of one or two environmental cations is taken into account. Therefore, the reason of large discrepancy with the experimental data for the population of the quartet S = 3/2 state with the temperature increase is an artefact of calculating the energy difference using the PBE functional at intramolecular charge transfer. This is because the contribution to the electron-electron interaction energy at long interelectron distances in this functional is described with a large error. The use of a correcting function, in which the density functional is used only for the calculations of the short-range contribution from the electron-electron interactions, allows one to eliminate this disadvantage. Using the improved HSEH1PBE (HSE06) functional, the energies of the S = 1/2 and 3/2 states were calculated using the optimized geometries of the corresponding complexes. Their difference, taking into account the contribution of a zero-point vibration energy according to the PBE calculation, is 79 meV and is in agreement with the experimental data (750 K or 65 meV).

The structures of isolated complexes $\{Cu^{II}(TPP^{2-})\}^{0}$ with S = 1/2 spin state, $\{Cu^{II}(TPP^{\bullet 3-})\}^{-}$ with S = 1 spin state, and the $\{Cu^{II}(TPP^{4-})\}^{2-}$ dianions with the ground S = 1/2 and excited S = 3/2 spin states are shown in Fig. S13a-S13d, respectively. Comparison of the lengths of the Cu-N and C-C bonds of the macrocycle (see Table S3) with the experimental data (Table 2) for the dianion shows a stronger discrepancy than that for the anionic complexes of nickel. Since these parameters are also noticeably different for two structurally nonequivalent $\{Cu^{II}(TPP^{4-})\}^{2-}$ dianions in the crystalline environment, this is indirect evidence of that stronger Coulomb interactions between cations and dianions in the crystal structure lattice affect significantly the geometry of the macrocyclic ligand. The ground state of $\{Cu^{II}(TPP^{4-})\}^{2-}$ is doublet S = 1/2 one, in accordance with the experiment. Comparison of charges and spin densities for the neutral (0.210, 0.568), anionic (0.193, 0.573), and dianionic complexes (0.123, 0.400) shows that both first and second electrons are transferred to the macrocycle at the reduction, and the d^9 electronic configuration of the Cu^{II} atoms remains unchanged.

In the quartet S = 3/2 state, which is 0.18 eV higher, charge and electron density on the Cu atom are 0.123 and 0.568, respectively. Therefore, electronic configuration d^9 of Cu^{II} is retained and transition of the macrocyclic ligand from singlet to triplet state occurs. It is not surprising that affinities for one (1.78 eV) and two (0.75 eV) electrons of the $\{Cu^{II}(TPP^{2-})\}^{0}$ complex coincide with such values for H_2TPP, 1.80 and 0.76 eV, respectively. The reason for the retention of electronic configuration of the metal atom during the

reduction of the copper complex is the disadvantage of the doubly populated x^2-y^2 orbital, which has an antibonding metal-ligand character, as well as the formation of an uncharacteristic planar-square environment of Cu^{I} formed during the reduction of the metal center. Rather great difference in the energies of the $\{Cu^{II}(TPP^{4-})\}^{2-}$ dianions with S = 1/2 and 3/2 spin states indicates that quartet state is not populated at room temperature in accordance with the experimental data.

The structure of isolated $\{Fe^{II}(TPP^{2-})\}^{0}$ and $\{Fe^{I}(TPP^{2-})\}^{-}$ species with the ground S = 1 and 1/2 states is shown in Figs. S13e and S13f, respectively. Decrease in charge on the metal atom by 0.058 is comparable with the value found previously for $\{Ni^{I}(TPP^{2-})\}^{-}$ indicating a change in the oxidation state of Fe from II to I at the reduction. Charge and spin density on the metal atom are 0.156 and 1.874, respectively, in the anionic $\{Fe^{I}(TPP^{2-})\}^{-}$ complex with S = 1/2 spin state. In the excited quartet S = 3/2 spin state, which is 0.30 eV higher in energy, spin density increases to 2.153 and, due to the population of the x^2-y^2 orbital, and charge increases to 0.197. In this case, the formation of high-spin state is not associated with intramolecular charge transfer. The macrocycle is symmetric in an isolated $\{Fe^{I}(TPP^{2-})\}^{-}$ anion (Table S2). This is consistent with the electronic configuration of the Fe^{I} atom - a filled block of d_{π} orbitals and one electron is positioned in a totally symmetric z^2 orbital. Therefore, slight alternation of bonds observed in the crystal of **4** (Table 2) can be associated most probably with asymmetry of the crystal environment.

Due to great number of atoms in the tetraphenylporphyrin complexes, purely technical limitations arise in the calculations of the number of optical transitions by the TD-DFT method. Therefore, only the long-wavelength part of the spectrum was investigated. It is interesting to compare Ni and Fe complexes which have the same oxidation state of metal atoms but rather different spectra in the long wave range. Transitions have been found in the near-IR range at 1179 and 1069 nm with noticeable oscillator strength of 0.025 and 0.015, respectively, for the Ni^{I} complex. This is in agreement with the experimental data (bands at 854 and 774 nm, Fig. 3b). At the same time Fe^{I} complex has two transitions at 877 nm with the 0.009 oscillator strength. These results in the shift of the absorption edge by about 200 nm towards shorter wavelengths are in full agreement with the experimental data.

Experimental

Materials.

Copper(II) 5, 10, 15, 20-tetraphenylporphyrin (Cu^{II}TPP, >98%), nickel(II) 5, 10, 15, 20-tetraphenylporphyrin (Ni^{II}TPP, >98%), and iron(III) chloride 5, 10, 15, 20-tetraphenylporphyrin (Fe^{III}ClTPP, >98%) were purchased from Porphychem. Cryptand[2.2.2] and anthracene (>99%) were purchased from Acros. Tributylmethylphosphonium iodide (Bu_3MePI, >98%) was purchased from TCI reagents. Cesium anthracenide was obtained according to Ref. 12. Iron(II) 5, 10, 15, 20-tetraphenylporphyrin was obtained by the reduction of Fe^{III}TPPCl with $NaBH_4$ in ethanol in anaerobic conditions according to Ref. 26. Toluene ($C_6H_5CH_3$, Acros) and *n*-hexane were distilled over Na/benzophenone in argon atmosphere. Solvents were degassed and stored in an MBraun 150B-G glove box. Salts **1** - **4** were synthesized and stored in a glove box with controlled atmosphere containing less than 1 ppm of water and oxygen. KBr pellets used for the IR and UV-visible-NIR analyses were prepared in a glove box. Magnetic measurements on SQUID and EPR were performed on a polycrystalline samples of **1** and **2** sealed in a 2 mm quartz tubes under ambient pressure of argon. Similar measurements were also carried out for a sealed sample of **3** but response on SQUID was too noisy due to insufficient amount of the sample.

General.

UV-visible-NIR spectra were measured in KBr pellets on a PerkinElmer Lambda 1050 spectrometer in the 250-2500 nm range. FT-IR spectra were obtained in KBr pellets with a PerkinElmer Spectrum 400 spectrometer (400-7800 cm^{-1}). EPR spectra were recorded for a polycrystalline sample of **1** - **3** from room temperature (295 K) down to liquid helium temperature with a JEOL JES-TE 200 X-band ESR spectrometer equipped with a JEOL ES-CT470 cryostat. A Quantum Design MPMS-XL SQUID magnetometer was used to measure static magnetic susceptibilities of **1** - **3** at 100 mT magnetic field in the cooling and heating conditions in the 300 – 1.9 K range. A sample holder contribution and core temperature independent diamagnetic susceptibility (χ_d) were subtracted from the experimental data. The χ_d values were estimated by the extrapolation of the data in the high-temperature range by fitting the data with the following expression: $\chi_M = C/(T - \Theta) + \chi_d$, where C is Curie constant and Θ is Weiss temperature. Effective magnetic moment (μ_{eff}) was calculated with the following formula: $\mu_{eff} = (8 \cdot \chi_M \cdot T)^{1/2}$

Table 3. X-ray diffraction data for **1**-**4**.

Compound	**1**	**2**	**3**	**4**
Emp. formula	$C_{160}H_{200}Cs_4Cu_2N_{16}O_{24}$	$C_{69}H_{72}CsN_6Ni\ O_6$	$C_{64}H_{66}N_4NiP$	$C_{64}H_{66}FeN_4P$
M_r [g·mol^{-1}]	3390.07	1272.94	980.88	978.02
Color and shape	Dark black block	Dark black block	Dark black block	Dark black block
Crystal system	monoclinic	monoclinic	monoclinic	monoclinic
Space group	P $2_1/c$	P $2_1/c$	P $2_1/c$	P $2_1/c$
a, Å	20.0683(2)	13.1280(1)	13.0766(4)	12.9989(13)
b, Å	43.0660(5)	16.7750(1)	17.4210(3)	17.5588(12)
c, Å	17.5575(2)	27.6823(3)	27.8842(10)	27.870(3)
α, °	90	90	90	90
β, °	94.816(1)	102.250(1)	126.742(5)	126.986(16)
γ, °	90	90	90	90
V, Å^3	15120.7(3)	5957.45(9)	5090.3(4)	5081.2(12)
Z	4	4	4	4
ρ_{calc} [g/cm^3]	1.489	1.419	1.281	1.278
μ [mm^{-1}]	1.305	0.987	0.459	0.374
F(000)	6968	2636	2084	2076
T [K]	100(2)	100(2)	100(2)	100(2)
Max. 2Θ, °	54.206	61.420	59.392	54.996
Reflns meas.	83385	38728	39961	36785
Unique reflns	32866	16662	12628	11350
Parameters	1877	749	679	659
Restraints	22	0	9	3
Reflns[F_o>2(F_o)]	27979	14601	8428	5297
R_1 [F_o>2σ(F_o)]	0.0359	0.0262	0.0592	0.0803
WR_2 (all data)[a],	0.0901	0.0594	0.1230	0.1984
G.O.F	1.052	1.033	1.060	1.051
CCDC number	2098888	2098887	2098886	2098885

Synthesis.

Crystals of $\{cryptand(Cs^+)\}_2\{Cu^{II}(TPP^{4-})\}^{2-}$ (**1**) were obtained via the reduction of $Cu^{II}TPP$ (28.2 mg, 0.042 mmol) by 2.16 equivalents of cesium anthracenide $(Cs^+)(C_{14}H_{10}^{\bullet-})$ (28 mg, 0.091 mmol) in the presence of two equvalents of cryptand (32 mg, 0.084 mmol) in 18 mL of toluene upon stirring at 80°C during 24 hours. Crystals of $\{cryptand(Cs^+)\}\{Ni^{I}(TPP^{2-})\}^- \cdot C_6H_5CH_3$ (**2**) were obtained by similar procedure. The reduction of $Ni^{II}TPP$ (28.2 mg, 0.042 mmol) by a cesium anthracenide $(Cs^+)(C_{14}H_{10}^{\bullet-})$ (14 mg, 0.0452 mmol) was carried out in the presence of one equvalent of cryptand (16 mg, 0.042 mmol) in 18 mL of toluene upon stirring at 80°C during 24 hours. The color of the solutions changed from red to deep red (**1**) and reddish-green (**2**) and metal(II) tetraphenylporphyrin completely dissolved.

For the synthesis of $(Bu_3MeP^+)\{Ni^{I}(TPP^{2-})\}^- \cdot C_6H_5CH_3$ (**3**) and $(Bu_3MeP^+)\{Fe^{I}(TPP^{2-})\}^- \cdot C_6H_5CH_3$ (**4**) reduction of $Ni^{II}TPP$ (28.2 mg, 0.042 mmol) for **3** and $Fe^{II}TPP$ (28.1 mg, 0.042 mmol) for **4** was carried out by a cesium anthracenide $(Cs^+)(C_{14}H_{10}^{\bullet-})$ (14 mg, 0.0452 mmol) in the presence of one equvalent of tributylmethylphosphonium iodide (14.4 mg, 0.042 mmol) in 18 mL of toluene upon stirring at 80°C during 24 hours. The color of the solutions changed from red to reddish-green for **3** and remained almost unchanged for **4,** and metal(II) tetraphenylporphyrins dissolved.

The obtained solutions were cooled down to room temperature and filtered into the 1.8-cm-diameter 50 mL glass tube with a ground glass plug, and then 24 mL of *n*-hexane was layered over the solution. Slow mixing of the solutions over 1.5 months resulted in precipitation of crystals. The solvent was then decanted from the crystals, and they were washed with *n*-hexane. Black blocks were obtained for both **1** and **2** in high yield (77 and 71%, respetively). Crystals were obtained in case of **3** and **4** as black blocks but yields of pure crystals were rather low, about 1 mg for **3** and only several small crystals for **4**. The composition of the obtained compounds was determined from X-ray diffraction analysis on a single crystal. Several crystals from one synthesis were found to consist of a single crystalline phase. Elemental analysis could not be used to confirm the composition of **1-4** due to their extremely high air-sensitivity.

X-ray crystal structure determination.

X-ray diffraction data for **1-4** were collected on an Oxford diffraction "Gemini-R" CCD diffractometer with graphite monochromated MoK_α radiation using an Oxford Instrument Cryojet system. Raw data reduction to F^2 was carried out using CrysAlisPro, Oxford Diffraction Ltd. The structures (Table 3) were solved by direct method and refined by the full-matrix least-squares method against F^2 using SHELX 2018/3 and Olex2 1.2.[27] Non-hydrogen atoms were refined in the anisotropic approximation. In the crystal structure of **1** one $–CH_2-CH_2-O-$ fragment of cryptand is disordered between two positions with the 0.709(5)/0.291(5) occupancies. All three butyl substituents in the Bu_3MeP^+ cation in **3** are disordered between two orientations with the 0.529(6)/0.471(6), 0.864(4)/0.156(4), 0.846(4)/0.154(4) occupancies. In the crystal structure of **4** one of three butyl substituents in the Bu_3MeP^+ cation is disordered between two orientations with the 0.536(6)/0.464(6) occupancies.

Conclusion

Metal tetraphenylporphyrins, where metal is copper(II), nickel(II) or iron(II) are reduced by cesium anthracenide. Crystalline products are obtained allowing one to study for the first time structure and properties of the $\{Cu^{II}(TPP^{4-})\}^{2-}$ dianions and the $\{Ni^{I}(TPP^{2-})\}^-$ anions. It is shown that reduction of $\{Cu^{II}(TPP^{2-})\}^0$ is centred exlusively on the macrocycle providing the fomation of TPP^{4-}. This macrocycle is diamagnetic and shows essential alternation of the C_{meso}-C bonds as well as the C-C bonds in the pyrrole rings. Cationic surrounding also affectes this alternation. New bands appear in the NIR spectrum of **1** due to population of LUMO at the formation of TPP^{4-}, and new transitions from this LUMO to above located orbitals become possible. Unpaired S = 1/2 spin is localized exclusively on the Cu^{II} atoms. Previously it was shown that second reduction of $\{Cu^{II}(TPP^{2-})\}^0$ in solution is also centred on the porphyrin macrocycle to form TPP^{4-}.[9b] On the contrary, one-electron reduction of $\{Ni^{II}(TPP^{2-})\}^0$ is metal-centered to yield the $\{Ni^{I}(TPP^{2-})\}^-$ anions at 100(2) K with unpaired S = 1/2 spin localized on Ni^{I}. That is confirmed by broad asymmetric EPR signals characteristic of Ni^{I} for both **2** and **3**. Correspondingly, dianionic TPP^{2-} macrocycles observed at 100(2) K show no alternation of bonds and do not contribute to the EPR signal. Existance of low-lying excited state is supposed for the $\{Ni^{I}(TPP^{2-})\}^-$ anions based on DFT calculations. This is charge transfer state whose formation is accomanied by electron transfer from Ni^{I} to TPP^{2-} yielding the $\{Ni^{II}(TPP^{\bullet3-})\}^-$ anions with a quartet S = 3/2 spin state. Therefore, the increase in magnetic moment of **2** above 150 K is attributed to population of the excited quartet state. Such transition is rather rare for metallomacrocycles. High-temperature behaviour of **2** and **3** above 150 K associated with broadened EPR signals agrees with the formation of two paramagnetic species having strong exchange interaction. Optical absorption bands characteristic of $TPP^{\bullet3-}$ are also manifested in the spectra of **2** and **3** at room temperature supporting the supposed transition. It should be noted that electrochemical reduction of $\{Ni^{II}(TPP^{2-})\}^0$ studied previously in solution shows macrocycle-centered reduction due to the appearance of EPR signal with g = 2.007 characteristic of $TPP^{\bullet3-}$. Nevertheless, similar transitions accociated with electron transfer between macrocycles and central nickel atoms were previusly observed in solutions for oxidized nickel(II) porphyrins. In this case according to optical spectra first oxidation is metal-centered for $\{Ni^{II}[(p\text{-Cl})TPP^{2-}]\}^0$ to form $\{Ni^{III}[(p\text{-Cl})TPP^{2-}]\}^+$ below 150 K but electron is transferred from macrocycle to nickel atom to form $\{Ni^{II}[(p\text{-Cl})TPP^{\bullet-}]\}^{\bullet+}$ when temperature rises above 150 K.[9a] Experimental data obtained for reduced $\{Fe^{II}(TPP^{2-})\}^0$ justify metal-centred reduction of this porphyrin accompanied by the formation of the $\{Fe^{I}(TPP^{2-})\}^-$ anions. This follows from weak alternation of the bonds in the macrocycle and the absence of any bands of $TPP^{\bullet3-}$ in the NIR spectrum of **4** at room temeperature. Nevertheless, this is not enough to support unambigously the formation of $\{Fe^{I}(TPP^{2-})\}^-$. Further investigations are needed involving magnetic measurements on SQUID and EPR. This work is planned in future. Nevertheless, the new method for preparation of metal porphyrin anions is developed allowing us to study for the first time their molecular structures, optical and magnetic properties in solid state. Some of these anions demostrate an interesting phenomenon such as magnetic transtions from low- to high-spin state accociated with metal to macrocycle charge transfer.

Conflicts of interest

There are no conflicts to declare.

Acknowledgements

The work was supported by Russian Science Foundation (project N 17-13-01215Π). Investigation of IR spectra of **1**-**4** was supported by the Ministry of Science and Higher education of the Russian

Federation (registration number AAAA-A19-119092390079-8). Some of the magnetic measurements were suported by JSPS KAKENHI Grant Number JP20K05448, and the JST (ACCEL) 27 (100150500010) project.

References

1 (a) The colors of life: an introduction to the chemistry of porphyrins and related compounds. L. R. Milgrom, Oxford University Press, Oxford, 1997, pp. 249; (b) T. Mashiko and D. Dolphin, *in Comprehensive Coordination Chemistry*, S. G. Wilkinson (ed.), Pergamon, Oxford, **1987**, *2*, 813–898.

2 (a) *The Porphyrin Handbook*; K. M. Kadish, K. M. Smith, R. Guilard (eds.), Academic Press, San Diego, 2010, **1–14**; (b) D. Wöhrle, G. Schnurpfeil, S. G. Makarov, A. Kazarin and O. N. Suvorova, *Macroheterocycles*, 2012, **5**, 191–202.

3 (a) J. L. Petersen, C. S. Schramm, D. R. Stojakovic, B. M. Hoffman and T. J. Marks, *J. Am. Chem. Soc*. 1977, **99**, 286–288; (b) H. Hasegawa, T. Naito, T. Inabe, T. Akutagawa and T. Nakamura, *J. Mater. Chem*. 1998, **8**, 1567–1570; (c) M. Matsuda, T. Naito, T. Inabe, N. Hanasaki, H. Tajima, T. Otsuka, K. Awaga, B. Narymbetov and H. Kobayashi, *J. Mater. Chem*. 2000, **10**, 631–636; (d) E. Tosatti, M. Fabrizio, J. Tóbik and G. E. Santoro, *Phys. Rev. Lett*. 2004, **93,** 117002. (e) T. Inabe and H. Tajima, *Chem. Rev*. 2004, **104**, 5503–5534; (f) J. S. Miller, C. Vazquez, J. C. Calabrese, M. L. McLean and A. J. Epstein, *Adv. Mater*. 1994, **6**, 217–221; (g) D. K. Rittenberg, L. Baars-Hibbe, A. B. Böhm and J. S. Miller, *J. Mater. Chem*. 2000, **10**, 241–244.

4 (a) D. Schaming, A. Giraudeau, L. Ruhlmann, C. Allain, J. Hao, Y. Xia, R. Farha, M. Goldmann, Y. Leroux and P. Hapiot, *IntechOpen,* E. Schab-Balcerzak (Ed.), 2011, 53–76. DOI: 10.5772/29086; (b) K. M. Morehouse, H. J. Sipe Jr. and R. P. Mason, *Arch. Biochem. Biophys.,* 1989, **273**, 158–164; (c) S. Kouno, A. Ikezaki, T. Ikeue and M. Nakamura, *J. Inorg. Biochem*. 2011, **105**, 718–721; (d) T. M. Swager and Y. Li, *Synfacts*, 2016; **12**, 1146. DOI: 10.1055/s-0036-1589381.

5 (a) K. M. Kadish, G. Royal, E. van Caemelbecke and L. Gueletti, in *The Porphyrin Handbook*; K. M. Kadish, K. M. Smith and R. Guilard (Eds.); Academic Press: San Diego, CA (USA), 2000, **9**, 1–219; (b) H. Kon, K. Tsuge, T. Imamura, Y. Sasaki, S. Ishizaka and N. Kitamura, *Inorg. Chem*. 2006, **45**, 6875–6883.

6 D. V. Konarev, A. V. Kuzmin, S. S. Khasanov, A. F. Shestakov, E. I. Yudanova, A. Otsuka, H. Yamochi, H. Kitagawa, R. N. Lyubovskaya, *J. Org. Chem*., 2018, **83**, 1861–1866.

7 D. V. Konarev, A. V. Kuzmin, S. S. Khasanov, A. F. Shestakov, D. I. Nazarov, A. Otsuka, H. Yamochi, H. Kitagawa and R. N. Lyubovskaya, *Eur. J. Inorg. Chem.*, 2020, 2615–2623.

8 (a) J. A. Cissell, T. P. Vaid and A. L. Rheingold, *Inorg. Chem.* 2006, **45**, 2367–2369; (b) J. A. Cissell, T. P. Vaid and A. L. Rheingold, *J. Am. Chem. Soc.* 2005, **127**, 12212–12213.

9 (a) D. Chang, T. Malinski, A. Ulman and K. M. Kadish, *Inorg. Chem*., 1984, **23**, 817–824; (b) Y. Fang, M. O. Senge, E. Van Caemelbecke, K. M. Smith, C. J. Medforth, M. Zhang and K. M. Kadish, *Inorg. Chem*., 2014, **53,** 10772−10778.

10 E. de Boer, Electronic structure of alkali metal adducts of aromatic hydrocarbons, *in Advances in Organometallic Chemistry*, F. G. A. Stone and R. West (Eds.), Elsevier, Academic Press Inc., 1964, Vol. **2**, pp. 115–157.

11 D. V. Konarev, A. V. Kuzmin, S. S. Khasanov, A. L. Litvinov, A. Otsuka, H. Yamochi, H. Kitagawa and R. N. Lyubovskaya, *Chem. Asian J.,* 2018, **13**, 1552–1560.

12 D. V. Konarev, A. V. Kuzmin, S. S. Khasanov, A. F. Shestakov, A. Otsuka, H. Yamochi, H. Kitagawa and R. N. Lyubovskaya, *Chem. Asian J.* 2020, **15**, 2689−2695.

13 A. L. Maclean, G. J. Foran, B. J. Kennedy, P. Turner and T.W. Hambley, *Aust. J. Chem.* 1996, **49**, 1273−1278.

14 L. Aparici Plaza, J. Chojnacki, *Acta Cryst. Sec. C: Cryst. Str. Commun.*, 2012, **68**, m24−m28.

15 N. Li, Z. Su, P. Coppens and J. Landrum, *J. Am. Chem. Soc*. 1990, **112**, 7294−7298.

16 T. Kaczmarzyk, T. Jackowski and K. Dziliński, *Nukleonika*, 2007, **52**, S99−S103

17 (a) D. V. Konarev, L. V. Zorina, S. S. Khasanov, E.U. Hakimova and R. N. Lyubovskaya, *New J. Chem*. 2012, **36**, 48−51; (b) D. V. Konarev, A. V. Kuzmin, S. V. Simonov, S. S. Khasanov, A. Otsuka, H. Yamochi, G. Saito and R. N. Lyubovskaya*, Dalton Trans*. 2012, **41**, 13841−13847; (c) D. V. Konarev, S. S. Khasanov, M. Ishikawa, A. Otsuka, H. Yamochi, G. Saito and R. N. Lyubovskaya, *Inorg. Chem*. 2013, **52,** 3851−3859; (d) D. V. Konarev, A. V. Kuzmin, S. S. Khasanov and R. N. Lyubovskaya, *Dalton Trans*. 2013, **42**, 9870−9876.

18 (a) D. V. Konarev, L. V. Zorina, M. Ishikawa, S. S. Khasanov, A. Otsuka, H. Yamochi, G. Saito and R. N. Lyubovskaya, *Cryst. Groth Des*. 2013, **13**, 4930−4939; (b) D. V. Konarev, A. V. Kuzmin, M. Ishikawa, Y. Nakano, M. A. Faraonov, S. S. Khasanov, A. Otsuka, H. Yamochi, G. Saito and R. N. Lyubovskaya, *Eur. J. Inorg. Chem.,* 2014, 3863−3870.

19 (a) M. A. Faraonov, N. R. Romanenko, A. V. Kuzmin, D. V. Konarev, A. F. Shestakov, P. A. Stuzhin, S. S. Khasanov, A. Otsuka, H. Yamochi, H. Kitagawa and R. N. Lyubovskaya, *Eur. J. Inorg. Chem.* 2019, 2918–2923; (b) M. A. Faraonov, N. R. Romanenko, A. V. Kuzmin, D. V. Konarev, S. S. Khasanov and R. N. Lyubovskaya, *Macroheterocycles,* 2019, **12** , 202–208.

20 C. Römelt, J. Song, M. Tarrago, J. A. Rees, M. van Gastel, T. Weyhermüller, S. DeBeer, E. Bill, F. Neese and S. Ye, *Inorg. Chem.* 2017, **56**, 4745–4750.

21 (a) D. V. Konarev, A. V. Kuzmin, M. A. Faraonov, M. Ishikawa, Y. Nakano, S. S. Khasanov, A. Otsuka, H. Yamochi, G. Saito and R. N. Lyubovskaya, *Chem. Eur. J.* 2015, **21**, 1014–1028; (b) D. V. Konarev, M. A. Faraonov, A. V. Kuzmin, S. S. Khasanov, Y. Nakano, M. S. Batov, S. I. Norko, A. Otsuka, H. Yamochi, G. Saito and R. N. Lyubovskaya, *New J. Chem.* 2017, **41**, 6866–6874; (c) D. V. Konarev, S. S. Khasanov, A. V. Kuzmin, Y. Nakano, M. Ishikawa, A. Otsuka, H. Yamochi, G. Saito and R. N.Lyubovskaya, *Inorg. Chem.* 2017, **56**, 1804–1813; (d) D. V. Konarev, M. A. Faraonov, M. S. Batov, M. G. Andronov, A.V. Kuzmin, S. S. Khasanov, A. Otsuka, H. Yamochi, H. Kitagawa and R. N. Lyubovskaya, *Dalton Trans.* 2020, **49**, 16821–16829.

22 (a) J. Telser, Y.-C. Fann, M. W. Renner, J. Fajer, S. Wang, H. Zhang, R. A. Scott and B. M. Hoffman, *J. Am. Chem. Soc.* 1997, **119***,* 733 – 743; (b) J. Telser, *J. Braz. Chem. Soc*. 2010, **21**, 1139–1157.

23 D. I. Nazarov, M. K. Islyaikin, E. N. Ivanov, O. I. Koifman, M. S. Batov, L. V. Zorina, S. S. Khasanov, A. F. Shestakov, E. I. Yudanova, Y. A. Zhabanov, D. A. Vyalkin, A. Otsuka, H. Yamochi, H. Kitagawa, T. Torres and D. V. Konarev, *Inorg. Chem*. 2021, **60**, 9857−9868.

24 (a) J. A. Cissell, T. P. Vaid and G. P. A. Yap, *J. Am. Chem. Soc.* 2007, **129**, 7841–7847; (b) D. V. Konarev, A. V. Kuzmin, A. F. Shestakov, S. S. Khasanov and R. N. Lyubovskaya, *Dalton Trans*, 2019, **48**, 4961–4972; (c) D. V. Konarev, A. V. Kuzmin, S. S. Khasanov, A. Otsuka, H. Yamochi, H. Kitagawa and R. N. Lyubovskaya, *Inorg. Chim. Acta*, 2020, **510**, 119732.

25 J. P. Perdew, K. Burke and M. Ernzerhof, *Phys. Rev. Lett*. 1996, **77**, 3865−3868.

26 (a) H. Kobayashi, Y. Yanagawa, *Bull. Chem. Soc. Jpn*, **1972**, *45*, 450−456; (b) B. B. Wayland, L. W. Olson and Z. U. Siddiqui, *J. Am. Chem. Soc.* 1976, **98**, 94−98 .

27 (a) G. M. Sheldrick, *Acta Crystallogr., Sect. A: Fundam. Crystallogr*. 2008, **64**, 112−122; (b) O. V. Dolomanov, L. J. Bourhis, R. J. Gildea, J. A. K. Howard and H. Puschmann, *J Appl .Crystallogr*, 2009, **42**, 339−341.